# Generalized framework of weak-value amplification in path interference of polarized light for the enhancement of all possible polarization anisotropy effects

Niladri Modak,[1,*] Athira B S,[2] Ankit Kumar Singh,[1] and Nirmalya Ghosh[1,2]

[1]*Department of Physical Sciences, Indian Institute of Science Education and Research (IISER) Kolkata, Mohanpur 741246, India*

[2]*Center of Excellence in Space Sciences India, Indian Institute of Science Education and Research (IISER) Kolkata, Mohanpur 741246, India*

(Received 16 June 2020; revised 19 April 2021; accepted 23 April 2021; published 19 May 2021)

Using the profound interferometric philosophy of weak-value amplification, we propose a simple, general, and robust polarization method for the amplification and quantification of small magnitudes of all possible polarization anisotropy effects in a single experimental embodiment. The approach is experimentally realized by introducing a weak coupling between the polarization degree of freedom of light and the path degree of freedom in a Mach-Zehnder interferometer in the presence of a weak anisotropy effect. Real and imaginary weak-value amplifications of different polarization anisotropy effects are manifested as characteristic changes in the relevant Stokes vector elements at the exit port of the interferometer, which follow orthogonal trajectories in the Poincaré sphere. The proof-of-concept experiment demonstrates that by using this scheme, one can faithfully extract and quantify an anisotropy parameter that is smaller than the typical sensitivity of measurement of a given Stokes parameter of a traditional polarimeter by a large weak-value amplification factor. This opens up the possibility of a sample measuring *weak-value polarimeter* for studying the rich variety of fundamental optical effects and for materials characterization and precision metrology.

DOI: 10.1103/PhysRevA.103.053518

## I. INTRODUCTION

Polarized light measurements have played a vital role in understanding and developing various advanced concepts of electromagnetic waves, and in numerous applications in diverse fields ranging from astronomy, materials characterization, biomedical imaging, remote sensing, to meteorology [1–7]. Polarimetry techniques probe the anisotropic polarizability of matter through the so-called birefringence (retardance) and dichroism (diattenuation) parameters [6–9]. These are traditionally quantified through exhaustive measurements of the $4\times4$ sample Mueller matrix or by multiple measurements of the $1\times4$ Stokes vector elements of sample-emerging light [6–9]. These conventional polarimetry techniques are, however, compromised when one needs to measure extremely small polarization effects desirable for certain applications, e.g., for the detection of physiological glucose concentration in human tissue, for the quantification of extremely small circular dichroism of proteins, for the determination of weak magneto-optical rotation in nanomaterials, and so on [6–9]. Measurements employing polarization modulation and synchronous detection have thus been developed [6–9]. Despite the availability of such different advanced techniques, there is a renewed recent interest in developing polarization methods that are particularly founded on the rich fundamental principle of wave optics, are technically simple, can obviate tedious measurements and calibration procedures, and yet are capable of providing high accuracy and sensitivity. Such methods are of both fundamental and applied interests, e.g., for studying a rich variety of spin (polarization) optical effects and various intriguing quantum optical phenomena, for the characterization of weakly anisotropic materials, and for precision metrology [2,4–12].

Despite being developed in the field of quantum mechanics [11,13–15], in recent times, weak measurements and weak-value amplification (WVA) have proven to be fundamentally important and extremely useful in the realm of both classical and quantum physics [16–33] due to their origin in wave interference [13–16]. The WVA mechanism using postselected weak measurements [34] has attracted particular attention in the optical domain for addressing fundamental questions [5,18,22,27–29,35,36] as well as for potential applications [18–20,24,25,29–33]. The WVA protocol sequentially involves the preparation of a system state (preselection), a weak coupling between the system and a pointer, and a postselection [11,13–15]. The near mutual orthogonal pre- and postselection of states gives rise to near destructive interference between the slightly separated pointer profiles leading to a large deflection of the resultant pointer profile, which is interpreted as the WVA of an observable [11,13–15]. WVA has been successfully used in classical optics for numerous practical applications, e.g., to amplify and detect tiny optical beam deflections [20] and spin Hall shifts of light [5,17], for the sensitive estimation of angular rotation [18], for high-resolution phase and frequency measurements [19,30], for the measurement of ultrasmall time delays, etc. Weak measurements have also been widely explored in the quantum optics domain [26–28,37].

In the context of polarization measurements, interesting weak measurement protocols have been developed for the determination of the quantum weak values of a single photon's

*nm16ip018@iiserkol.ac.in

 ©2021 American Physical Society

polarization [32,38], for the direct measurement of the general polarization state of light [29], or to perform polarization state tomography of light fields [36]. These measurement schemes are aimed at finding out the weak values of the Stokes polarization operators of single-photon or classical light beams [32,38]. While several weak measurement protocols have been developed for the characterization of the polarization state of light, a relatively lesser amount of research has been done for the extraction and quantification of small polarization anisotropy properties of a sample [30,31,33,39]. In a recent study, the optical activity of a sample was probed by high-precision measurements of the changes in the amplitude and the phase of a light beam via the measurement of both real and imaginary (respectively) weak values using different polarization state postselections [30]. In another weak measurement protocol, the optical rotation signal of a chiral sample was amplified and detected by introducing a weak coupling between the polarization and the spectral degree of freedom of light and by the subsequent pre- and postselection of states using appropriate polarizations [31]. Similarly, the optical polarization rotation was successfully amplified by adopting an angular version of the von Neumann measurement scheme [33]. Another useful technique that is worth mentioning here is the so-called quasi-null-polarization-detection method to amplify small optical rotatory dispersion signals from chiral samples [39]. Even though this is not a WVA scheme *per se*, in this method also, the chiral sample is illuminated with weakly elliptically polarized light and subsequent postselection is done in near orthogonal linear polarization. This essentially results in a large increase of the ratio of the chiral to the achiral signal intensity, leading to the amplification of the optical rotatory dispersion signal.

In this paper, we introduce a polarization measurement technique capable of amplifying and quantifying small magnitudes of all the polarization anisotropy effects of a sample based on the interferometric philosophy of postselected weak measurements [11,13]. In this approach, the near destructive interference of two paths in an interferometer serves the purpose of near orthogonal pre- and postselection of states [20] unlike conventional optical schemes of WVA. A weak polarization anisotropy effect introduced in one path of the interferometer provides the desirable weak coupling between the path degree of freedom and the polarization degree of freedom of light. The real and the imaginary WVAs of different anisotropy effects are manifested in different characteristic Stokes vector elements (acting as the pointer here) [8,9] at the exit port of the interferometer, enabling the quantification of all the anisotropy effects in the same experimental embodiment without involving any additional anisotropy effect-dependent postselections. Note that interferometric arrangements have also been used previously for obtaining weak-value amplification [20,40]. However, in most of those schemes the spatial degree of freedom of light (spatial mode) has been used as a pointer whereas the paths of the interferometric setup have been given two different polarizations. The WVA in such a scenario manifests as a large change in the pointer beam profile either in the spatial or in momentum space. In contrast, our scheme incorporates the polarization state of light itself as a pointer enabling the WVA of polarization anisotropy effects.

The paper is organized as follows. In Sec. II, we provide the theoretical framework for interferometric WVA of all the polarization anisotropy effects along with its corresponding classical field-based formalism. Section III provides the experimental details of interferometric WVA. In Sec. IV, the experimental and simulation results are presented and discussed. Section V concludes with an outlook on this type of weak-value polarimeter, its possible extension towards imaging and spectroscopic polarimetry, and its potential applications.

## II. THEORETICAL FORMALISM OF INTERFEROMETRIC WVA OF POLARIZATION ANISOTROPY EFFECTS

In this framework, the weak value of a given polarization anisotropy is realized through the near destructive interference of polarized light in an interferometer [see Fig. 1(a)]. Here, near destructive interference refers to the destructive interference of two fields having a phase difference $\pi$ with a small amplitude offset $\epsilon_a = \tan^{-1}(\frac{1-a}{1+a})$ ($a$ is the ratio of amplitudes of the two fields) or the interference of two fields having equal amplitude ($a = 1$) but with a phase difference of $\pi \pm 2\epsilon_p$ where $\epsilon_p$ is a small phase offset. The former generates *real* WVA and the latter *imaginary* WVA. The $\epsilon_{a/p}$ parameters are equivalent to the overlap of near orthogonal pre- and postselection states in weak measurements. We define the generalized polarization anisotropy parameter $\alpha$ in terms of the difference in the refractive index RI ($n$) between orthogonal linear or circular polarizations as $2\alpha = \frac{2\pi}{\lambda}(n^{r/i}_{L/C} - n^{r/i}_{L'/C'})t$. Here, $t$ is the path length, and the superscripts $r/i$ correspond to real/imaginary parts of RI, and the subscripts $L/C$ and $L'/C'$ represent linear/circular polarizations and their orthogonal states, respectively. The real/imaginary parts of RI generate amplitude/phase anisotropies and are associated with retardance/diattenuation effects, respectively [8,9]. We now derive an interferometric WVA framework based on the postselection-aided weak measurement formalism.

### A. Postselected weak measurement formalism

The weak coupling between the path degree of freedom (system) and polarization state (pointer) of a light beam in the interferometric arrangement [see Fig. 1(a)] can be expressed by the unitary evolution $U(\alpha) = e^{-i\alpha G\hat{A}}$ [11,13,41]. Here, the polarization anisotropy parameter $\alpha \to 0$, and $G$ is the generator of the polarization effect acting as the pointer variable [42]. It generates 2×2 Jones matrices corresponding to the different polarization anisotropy effects. Henceforth, we use the superscripts $\mathfrak{a}/\mathfrak{p}$ to describe amplitude/phase anisotropy effects in the corresponding generators $G^{\mathfrak{a}}_j = \frac{i}{2}\sigma_j$ and $G^{\mathfrak{p}}_j = \frac{1}{2}\sigma_j$, respectively, where $\sigma_j$ ($j = 1, 2, 3$) are the standard 2×2 Pauli matrices. In our context, the subscripts $j = 1, 2, 3$ are related to the generator for the Jones matrix corresponding to the anisotropy effects in the $\pm 45^\circ$ linear polarization, right-left circular polarization, and horizontal ($x$)-vertical ($y$) linear polarization basis, respectively [42]. The observable $\hat{A}$ representing the opposite polarization anisotropy effects $+\alpha$ and $-\alpha$ in the two paths (path $|1\rangle$ and path $|2\rangle$, respectively) of the interferometer can be expressed as a 2×2 diagonal matrix

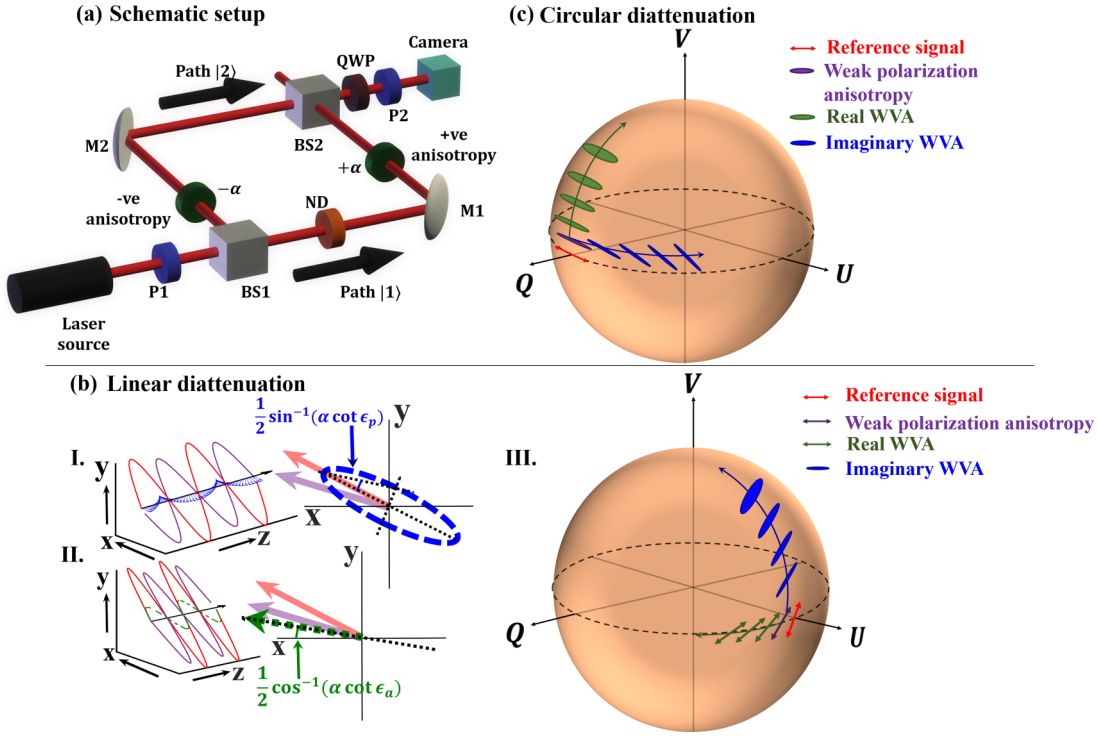


FIG. 1. (a) Schematic of the Mach-Zehnder interferometric arrangement for WVA of polarization anisotropy effects. (P1,P2): polarizers; QWP: quarter-wave plate; (BS1, BS2): 50:50 beam splitters; (M1, M2): mirrors; ND: variable neutral density filter. WVA of (b) linear diattenuation and (c) circular diattenuation. (b) Electric field vectors and polarization ellipse undergoing imaginary (I) and real (II) WVA are illustrated. I: Electric fields corresponding to the $+45^\circ$ polarized light in path 1 (red solid line), after experiencing a small linear diattenuation in path 2 (violet solid line) and the resultant field following near destructive interference with a small phase offset $\epsilon_p$ (blue dashed line) are depicted. Enhancement of ellipticity due to imaginary WVA is also displayed and the expression for ellipticity is noted. II: Corresponding electric fields for real WVA. The resultant field after near destructive interference with a small amplitude offset $\epsilon_a$ is shown (green dashed line). The change in the orientation angle of the electric field due to real WVA is also displayed and the corresponding expression is noted. III: Evolution of the Stokes vectors in the Poincaré sphere for real (green line) and imaginary (blue line) WVA of linear diattenuation. (c) Evolution of the Stokes vectors in the Poincaré sphere for real (green line) and imaginary (blue line) WVA of circular diattenuation.

$\hat{A} = |1\rangle\langle 1| - |2\rangle\langle 2| = \left[\begin{smallmatrix} 1 & 0 \\ 0 & -1 \end{smallmatrix}\right]$ [20]. The preselection ($|\psi_i\rangle$) and postselection ($|\psi_f\rangle$) of states can be obtained by the path degree of freedom as follows,

$$|\psi_i\rangle = \frac{1}{\sqrt{2}}[|1\rangle + |2\rangle], \tag{1a}$$

$$|\psi_f\rangle = \frac{1}{\sqrt{1+a^2}}[e^{\pm i\epsilon_p}|1\rangle - ae^{\mp i\epsilon_p}|2\rangle]. \tag{1b}$$

In the weak-coupling limit ($\alpha \to 0$), the final pointer state after postselection is obtained as [11,13–15]

$$|\phi_f\rangle \approx \langle\psi_f|\psi_i\rangle e^{-i\alpha G A_w}|\phi_i\rangle. \tag{2}$$

Here, $A_w = \frac{\langle\psi_f|\hat{A}|\psi_i\rangle}{\langle\psi_f|\psi_i\rangle}$ is the interferometric weak value of the operator $\hat{A}$. $|\phi_i\rangle$ is the initial pointer state, which is the input polarization state represented by the Jones vector. In this framework, the polarization transformation is determined by Eq. (2) and accordingly the final state will depend upon the values of $A_w$ and $\alpha$.

### *1. Real weak-value amplification*

Real WVA is obtained at the exact destructive interference position (a phase difference of $\pi$, $\epsilon_p = 0$) with a small amplitude offset $\epsilon_a$. Using Eqs. (1) and (2), the final pointer state after postselection is obtained as

$$|\phi_f\rangle \sim e^{-i\alpha\cot\epsilon_a G}|\phi_i\rangle. \tag{3}$$

Equation (3) implies an enhancement of the polarization anisotropy effect $\alpha$ by a factor $\cot\epsilon_a$, which is reflected in the final Jones vector pointer state.

### *2. Imaginary weak-value amplification*

Imaginary WVA is obtained by the near destructive interference of two paths with equal amplitude ($a = 1$) but with a phase offset $\epsilon_p$ from the exact destructive interference position. The final pointer state after postselection, in this case, becomes

$$|\phi_f\rangle \sim e^{\alpha\cot\epsilon_p G}|\phi_i\rangle. \tag{4}$$

Depending upon the anisotropy effect (described by generator $G$), the Jones vector pointer state will be characteristically modified.

For example, in the case of optical rotation $\alpha$, the pointer variable is expressed by $G_2^{\mathfrak{p}}$ with an input $x$-polarized state (Jones vector) as $|\phi_i\rangle = [1 \quad 0]^T$. Following Eq. (3), the real

WVA is obtained in the final pointer state $|\phi_f\rangle$,

$$|\phi_f\rangle \sim e^{-i\alpha \cot\epsilon_a G_2^{\mathrm{p}}}|\phi_i\rangle \sim \begin{bmatrix} \cos(\alpha\cot\epsilon_a) \\ -\sin(\alpha\cot\epsilon_a)\end{bmatrix}. \tag{5}$$

Clearly, from Eq. (5), the real WVA of a small optical rotation $\alpha$ is manifested as a large enhancement in the orientation angle ($=\alpha\cot\epsilon_a$) of the output Jones vector [9]. This is valid for the case $\epsilon_a \to 0$.

Similarly, using Eq. (4), the final state after postselection for an imaginary WVA of small optical rotation can be obtained as

$$|\phi_f\rangle \sim e^{i\alpha\cot\epsilon_p G_2^{\mathrm{a}}}|\phi_i\rangle \sim \begin{bmatrix} \cosh(\alpha\cot\epsilon_p) \\ -i\sinh(\alpha\cot\epsilon_p)\end{bmatrix}. \tag{6}$$

Imaginary WVA, in Eq. (6), is manifested as a large change in the ellipticity of the output Jones vector [9] with decreasing $\epsilon_p$.

The above formalism is a generalized one where all the different polarization anisotropy effects, namely, linear and circular diattenuation, and linear and circular retardance, are included in the framework. Note that the expressions for experimentally measurable Stokes vectors corresponding to the Jones vectors presented above can be easily worked out using the standard algebra connecting the Jones and Stokes formalism [9]. In what follows, we complement the above weak measurement formalism with its corresponding classical field-based analog. We also provide a more detailed account of real and imaginary WVAs of different polarization anisotropy effects and how they are manifested in the characteristic Stokes vector elements.

### B. Classical field-based formalism

#### 1. WVA of diattenuation

*Linear diattenuation (x-y).* The real and imaginary WVAs of the linear diattenuation effect can be modeled using Eqs. (3) and (4) using the generator $G_3^{\mathrm{a}}$, and input state $|\phi_i\rangle = \frac{1}{\sqrt{2}}[1 \quad 1]^T$ in the formalism described in the preceding section. In the classical field analog, this scenario can be mimicked through the interference of $+45^\circ$ polarized light in one path with a slightly changed polarization state after experiencing a small linear diattenuation effect between the horizontal ($x$) and vertical ($y$) polarization components in the other path. The corresponding electric fields are

$$\boldsymbol{E}_1 = \xi\frac{\hat{x}+\hat{y}}{\sqrt{2}}, \quad \boldsymbol{E}_2 = \xi\frac{e^{\alpha}\hat{x}+e^{-\alpha}\hat{y}}{\sqrt{e^{2\alpha}+e^{-2\alpha}}}. \tag{7}$$

$\xi$ is an arbitrary field amplitude factor. Note that the $+\alpha$ and $-\alpha$ effects in both paths, respectively (as mentioned in Sec. II A), are equivalent to the $2\alpha$ effect in a single path. The imaginary WVA can be obtained by a small phase offset $\epsilon_p$ from the exact destructive interference of $\boldsymbol{E}_1$ and $\boldsymbol{E}_2$ to yield the resultant field $\boldsymbol{E}$ as [13,16]

$$\boldsymbol{E} = (\cos\epsilon_p \pm i\sin\epsilon_p)\boldsymbol{E}_1 - (\cos\epsilon_p \mp i\sin\epsilon_p)\boldsymbol{E}_2. \tag{8}$$

Equations (7) and (8) can be used to obtain the expression for the corresponding Stokes vector elements ($S = [I\ Q\ U\ V]^T$) [8,9]. In the weak-coupling limit ($\alpha \to 0$) [11,13–15], the circular (elliptical) polarization descriptor fourth Stokes vector element ($\frac{V}{I}$) [8,9] can be shown to exhibit WVA with decreasing $\epsilon_p$ as

$$\frac{V}{I} \approx \mp\alpha\cot\epsilon_p. \tag{9}$$

The corresponding expressions for real WVA can be obtained by the destructive interference of $\boldsymbol{E}_1$ and $\boldsymbol{E}_2$ with a small amplitude offset $\epsilon_a$ ($=\tan^{-1}\frac{1-a}{1+a}$) to yield [13,16]

$$\boldsymbol{E} = (\cos\epsilon_a \pm \sin\epsilon_a)\boldsymbol{E}_1 - (\cos\epsilon_a \mp \sin\epsilon_a)\boldsymbol{E}_2. \tag{10}$$

Once again, in the weak-coupling limit ($\alpha \to 0$), the real WVA is manifested in the linear polarization descriptor Stokes vector element ($\frac{Q}{I}$) (for $\epsilon_a \to 0$) as

$$\frac{Q}{I} \approx \mp\alpha\cot\epsilon_a. \tag{11}$$

Complete expressions for the relevant Stokes vector elements ($V, I$ for imaginary WVA and $Q, I$ for real WVA) are provided in Appendix A. The electric fields and the polarization ellipse corresponding to the WVA of linear diattenuation are pictorially illustrated in Fig. 1(b). For real WVA, with varying $\epsilon_a$, the Stokes polarization state evolves in the Poincaré sphere along the geodesic trajectory connecting the states of the two paths of the interferometer (the input state and the state after encountering the weak anisotropy effect). For imaginary WVA, the corresponding trajectory with varying $\epsilon_p$ lies in a plane that is perpendicular to the geodesic trajectory [Fig. 1(b)(III)]. This appears to be a general rule for all the anisotropy effects.

*Circular diattenuation.* The real and imaginary WVAs of this effect can be modeled using Eqs. (3) and (4) with the generator matrix $G_2^{\mathrm{a}}$, and with the choice of the input state $|\phi_i\rangle = [1 \quad 0]^T$ in the weak-value formalism. In the classical field-based formalism, the corresponding expressions for the fields $\boldsymbol{E}_1$ and $\boldsymbol{E}_2$ for input horizontal ($x$) polarization are provided in Table I. This leads to imaginary and real WVAs (respectively) of circular diattenuation in the Stokes vector elements as

$$\frac{U}{I} \approx \alpha\cot\epsilon_p, \tag{12a}$$

$$\frac{V}{I} \approx \alpha\cot\epsilon_a. \tag{12b}$$

The exact expressions for the above Stokes vector elements are provided in Appendix A. The corresponding polarization state trajectories in the Poincaré sphere for varying $\epsilon_{a/p}$ are shown in Fig. 1(c).

#### 2. WVA of linear and circular retardance

The above framework for WVA can be generalized for retardance properties also (shown in Table I). Full expressions for the relevant Stokes vector elements are provided in Appendix A. From a fundamental point of view, it is interesting to note that the real and the imaginary WVAs of a given polarization anisotropy effect are manifested in different Stokes vector elements ($Q, U, V$), which act as conjugate variables. It is interesting to note the quantum mechanical equivalence where the corresponding quantum Stokes operators satisfy commutation relations and the respective variances

TABLE I. Real and imaginary WVAs of all the polarization anisotropy effects. The four different polarization anisotropy effects (first column), the corresponding input electric field and the electric field after experiencing a small anisotropy effect (second column), and the Stokes vector elements carrying signatures of real and imaginary WVAs of the respective anisotropy effects (third column). The polarization optical components used to experimentally realize the WVAs of the respective anisotropy effects are listed in the fourth column.

| | Electric fields | | Stokes vector elements | | |
|---|---|---|---|---|---|
| Anisotropy effects | $\frac{\boldsymbol{E}_1}{\xi}$ | $\frac{\boldsymbol{E}_2}{\xi}$ | Real WVA | Imaginary WVA | Polarization optical component |
| Linear diattenuation | | | | | |
| $(x-y)$ | $\frac{\hat{x}+\hat{y}}{\sqrt{2}}$ $+45^\circ$ linear polarization | $\frac{e^{\alpha}\hat{x}+e^{-\alpha}\hat{y}}{\sqrt{e^{2\alpha}+e^{-2\alpha}}}$ | $\frac{Q}{I}$ | $\frac{V}{I}$ | Linear polarizer oriented at a small angle from $+45^\circ$ |
| Circular diattenuation | $\hat{x}=\frac{\hat{r}+\hat{l}}{\sqrt{2}}$ Horizontal linear polarization | $\frac{e^{\alpha}\hat{r}+e^{-\alpha}\hat{l}}{\sqrt{e^{2\alpha}+e^{-2\alpha}}}$ | $\frac{V}{I}$ | $\frac{U}{I}$ | Quarter-wave plate with its optic axis oriented at a small angle from horizontal polarization |
| Linear retardance | $\frac{\hat{x}+\hat{y}}{\sqrt{2}}$ $+45^\circ$ linear polarization | $\frac{e^{i\alpha}\hat{x}+e^{-i\alpha}\hat{y}}{\sqrt{2}}$ | $\frac{V}{I}$ | $\frac{Q}{I}$ | Liquid-crystal variable retarder with small retardance |
| Optical rotation | $\hat{x}=\frac{\hat{r}+\hat{l}}{\sqrt{2}}$ Horizontal linear polarization | $\cos\alpha\hat{x}+\sin\alpha\hat{y}$ | $\frac{U}{Q}$ | $\frac{V}{I}$ | Chiral sample or half-wave plate oriented at small angle with respect to horizontal polarization |

are also restricted by uncertainty relations [43]. From a practical point of view, the manifestation of real and imaginary WVAs of various polarization anisotropy effects in characteristic Stokes vector elements open up the possibility of a weak-value polarimeter for the amplification and quantification of all the polarization anisotropy effects using a single experimental embodiment with relative experimental ease. We experimentally demonstrate this subsequently.

## III. EXPERIMENTAL REALIZATION OF SAMPLE-MEASURING WEAK-VALUE POLARIMETER

In our experiment, the 632.8-nm line of a He-Ne laser is passed through a rotatable polarizer (P1) and is used to seed the interferometer [see Fig. 1(a)]. The small polarization anisotropy effect is introduced in one arm using standard polarization optical elements noted in the fourth column of Table I. The light beams in the two arms with slightly different polarization states then interfere at the exit port and the resulting fringes are imaged into a CCD camera. The spatially resolved Stokes vector elements across the interference fringe are measured using a combination of a quarter-wave plate (QWP) and a linear polarizer (P2) [8,9]. The standard Stokes vector measurement procedure [8,9] was adopted for this purpose by performing six linear and circular polarization intensity measurements using QWP and P2, respectively; $I_H$: P2 at $0^\circ$ and QWP at $0^\circ$; $I_V$: P2 at $90^\circ$ and QWP at $90^\circ$; $I_P$: P2 at $45^\circ$ and QWP at $45^\circ$; $I_M$: P2 at $135^\circ$ and QWP at $135^\circ$; $I_R$: P2 at $0^\circ$ and QWP at $45^\circ$; $I_L$: P2 at $0^\circ$ and QWP at $135^\circ$ [8,9]. For the quantification of the imaginary WVA, the intensities in the two arms are kept equal (amplitude ratio $a=1$) and the spatial variation of the relevant Stokes vector elements around the position of the destructive interference intensity minima (corresponding to phase $\pi$) are recorded. Here, a single set of measurements of the spatial variations of the relevant Stokes vector element is sufficient. This spatial variation is used to generate its variation as a function of the small phase offset parameter (a phase shift of $\epsilon_p$ from $\pi$), which increases gradually as one moves away from the destructive interference point. Probing the real WVA, on the other hand, involves multiple sets of measurements of the spatial variation of the relevant Stokes vector elements. In order to quantify the real WVA, the relative intensities (or amplitude ratio $a$) of light in the two arms are varied using a variable neutral density filter (ND) [see Fig. 1(a)]. For each value of $a$, the measured Stokes polarization parameters corresponding to the spatial position of the destructive interference (intensity minima) are used to generate the variations of the relevant Stokes parameters with the small amplitude offset parameter $\epsilon_a$. The calibration procedure of our experimental system is discussed in Appendix B.

## IV. RESULTS AND DISCUSSION

First, we illustrate the WVA concept through the simulation of the interference experiment taking a small linear retardance ($\alpha = 0.017$ rad) as the weak polarization anisotropy effect and the corresponding results are shown in Fig. 2. For the simulations of the interference fringes and the corresponding imaginary and real WVAs of linear retardance, the electric fields $\boldsymbol{E}$ corresponding to Eqs. (8) and (10), respectively, are used by taking the expressions for $\boldsymbol{E}_1$ and $\boldsymbol{E}_2$ from the fourth row of Table I. The amplitude factor $\xi$ was taken to be a Gaussian (width = 1 mm) to mimic the light beam for the simulation of the interference fringes. The Stokes vector elements corresponding to these interfering fields were generated using standard Stokes algebra [8,9] and the corresponding expressions are provided in Eqs. (A10) and (A11) and Eqs. (A12) and (A13) of Appendix A for real and imaginary WVAs, respectively. As is apparent from Fig. 2(a), the $\frac{Q}{I}$

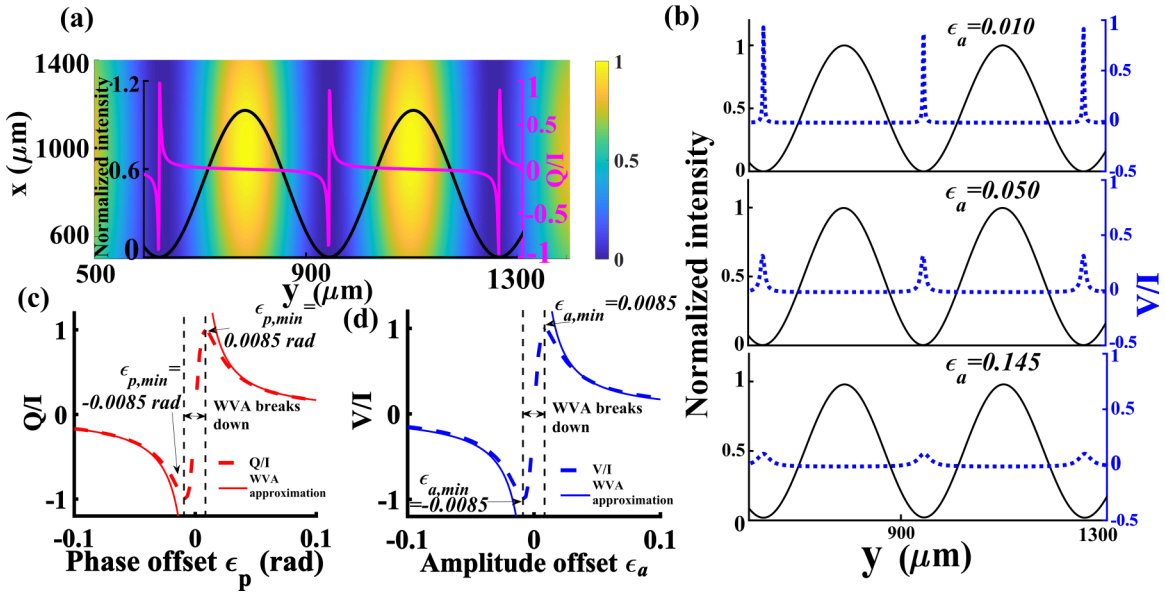


FIG. 2. Simulation of real and imaginary WVAs of linear retardance ($\alpha = 0.017$ rad). (a) Typical fringe profile of the interference of $+45^\circ$ polarized Gaussian beam (width = 1 mm) with another beam having a slightly changed polarization state due to the weak linear retardance effect. The intensity profile (left axis, black line) and the spatial variation of the $\frac{Q}{I}$ Stokes parameter (right axis, magenta line) along the $y$ axis of the fringe are displayed. The color bar represents the magnitude of intensity. The $\frac{Q}{I}$ parameter exhibits imaginary WVA. (b) Corresponding results for real WVA. The intensity profile (left axis, black solid line) and spatial variations of the $\frac{V}{I}$ Stokes parameter (right axis, blue dashed line) are shown for three different values of the amplitude offset parameter $\epsilon_a = 0.010, 0.050, 0.145$. (c) Variation of $\frac{Q}{I}$ with the phase offset parameter $\epsilon_p$ (red solid circles) and corresponding theoretical fit to imaginary WVA ($\sim\alpha \cot \epsilon_p$) (red dashed line). (d) Variation of $\frac{V}{I}$ with $\epsilon_a$ (blue solid circles) and the real WVA fit ($\sim\alpha \cot \epsilon_a$, blue dashed line). The regions where the WVA approximation breaks down ($\epsilon_{a/p,\min} \lesssim \frac{\alpha}{2}$) are also marked.

Stokes parameter exhibits a prominent enhancement at close vicinity of the intensity minima of the destructive interference position. Accordingly, $\frac{Q}{I}$ increases rapidly as $\propto\alpha \cot \epsilon_p$ with a decreasing small phase offset parameter $\epsilon_p$ [Fig. 2(c)], implying the manifestation of the imaginary WVA of linear retardance $\alpha$. The corresponding real WVA of $\alpha$ is manifested in the $\frac{V}{I}$ Stokes parameter [see Figs. 2(b) and 2(d)]. The variations of the $\frac{V}{I}$ parameter across the fringe are shown for three different values of the small amplitude offset $\epsilon_a$ in Fig. 2(b). The $\frac{V}{I}$ parameter also increases rapidly with decreasing $\epsilon_a$ and varies as $\propto\alpha \cot \epsilon_a$ [Fig. 2(d)], implying a real WVA. However, as opposed to the approximate expressions, the exact magnitudes of the WVAs [obtained using Eqs. (A10) and (A11) and Eqs. (A12) and (A13) of Appendix A] saturate and start decreasing below a certain value of the $\epsilon_{p/a}$ parameters ($\epsilon < \epsilon_{\min}$), which are universal characteristics of WVA [11,13–15]. In accordance with this and as is evident from Figs. 2(c) and 2(d), there is a limiting value of amplification and a corresponding minimum value of $\epsilon_{p/a}$ ($\epsilon_{\min} \sim \frac{\alpha}{2}$) as in the conventional WVA. Here, the limits are set by the fundamental limit of degree of polarization ($\leqslant 1$). These limiting values of the $\epsilon_{p/a}$ parameters in both the regions $\epsilon_{p/a} > 0$ and $\epsilon_{p/a} < 0$ for imaginary and real WVAs are marked in Figs. 2(c) and 2(d), respectively. As $\epsilon_{p/a}$ approaches zero, the WVA approximation breaks down and the shift of the pointer profile also approaches zero, illustrating the nondiverging nature of WVA [Figs. 2(c) and 2(d)] [11,13–15].

The experimental results for linear ($x$-$y$) diattenuation (Fig. 3) reveal the role of the Stokes parameters $\frac{V}{I}$ and $\frac{Q}{I}$ in the imaginary and real WVAs of linear diattenuation, respectively, as opposite to the case of linear retardance. Accordingly, the $\frac{V}{I}$ parameter approaches its maximum value near the destructive interference intensity minima [see Fig. 3(b)]. The variation of $\frac{V}{I}$ with $\epsilon_p$ [Fig. 3(c)] shows good agreement with the corresponding imaginary WVA of linear ($x$-$y$) diattenuation ($\alpha = 0.051$) as predicted in Eq. (9) ($\propto\alpha \cot \epsilon_p$). Similarly, the $\frac{Q}{I}$ parameter also varies as $\propto\alpha \cot \epsilon_a$ [see Fig. 3(d)], as predicted by Eq. (11) for real WVA of linear diattenuation ($\alpha = 0.017$). While the imaginary WVA results [Fig. 3(c)] are extracted from a single spatial map of $\frac{V}{I}$, the real WVA results [Fig. 3(d)] are derived from multiple measurements of $\frac{Q}{I}$ for varying intensity ratios at the two arms. This makes the latter more prone to experimental errors. Theoretical predictions [using Eqs. (A2)–(A5) of Appendix A] of the imaginary and real WVAs of linear ($x$-$y$) diattenuation are shown in the insets of Figs. 3(c) and 3(d), respectively. Once again, the limiting behavior of the WVA is apparent when $\epsilon_{p/a}$ approaches the limit ($\epsilon_{\min} \sim \frac{\alpha}{2}$). In the experiments, the values for $\epsilon_{p/a}$ were always greater than this limiting value $\epsilon_{\min}$. The calibration procedure of the experimental system to extract the imaginary and real weak values (presented above) is discussed in Appendix B.

Figure 4 provides experimental results of WVA of circular diattenuation ($\alpha = 0.012$). The imaginary WVA is manifested as an increase of the $\frac{U}{I}$ Stokes parameter with decreasing $\epsilon_p$ [Fig. 4(a)] showing good agreement with the corresponding prediction [$\propto\alpha \cot \epsilon_p$, Eq. (12a)]. The real WVA [Fig. 4(b)] is manifested as the ($\propto\alpha \cot \epsilon_a$) variation of the $\frac{V}{I}$ Stokes

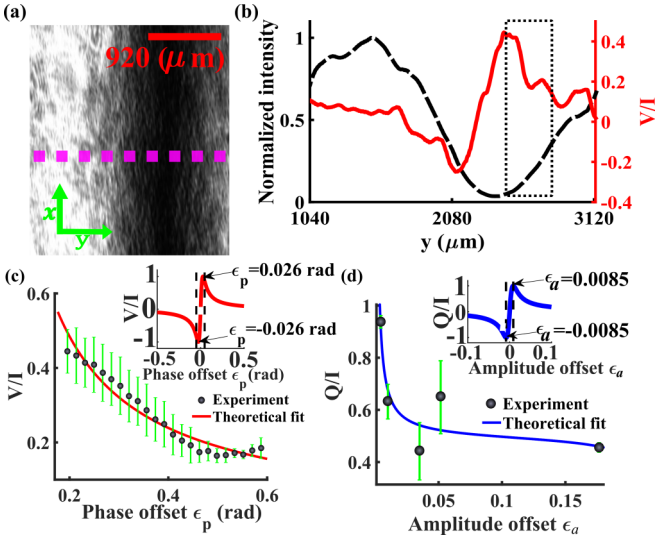


FIG. 3. Experimental results of real and imaginary WVAs of linear diattenuation. (a) Recorded fringe profile of the interference of a $+45^\circ$ polarized Gaussian beam with another beam having a $42^\circ$ polarization state due to the weak linear diattenuation effect $\alpha = 0.051$. (b) The intensity profile (left axis, black dashed line) and spatial variation of the $\frac{V}{I}$ Stokes parameter (right axis, red solid line) along the magenta dashed line mark in (a). The rapid variation of $\frac{V}{I}$ around the destructive interference position, shown in the black dotted box, is a manifestation of imaginary WVA. (c) Variation of $\frac{V}{I}$ as a function of $\epsilon_p$ (black circles) and theoretical fit to imaginary WVA ($\alpha \cot \epsilon_p$) (red line). For real WVA, we took $\alpha = 0.017$ by placing the linear polarizer at an angle $44^\circ$ with respect to the horizontal axis in one arm of the interferometer. (d) Variation of $\frac{Q}{I}$ as a function of $\epsilon_a$ (black circles) and the corresponding real WVA fit ($\alpha \cot \epsilon_a$, blue line). Error bars in (c) and (d) represent standard deviations. Corresponding theoretical predictions of imaginary and real WVAs along with the maximum enhancement limit (minimum $\epsilon_{p/a}$, i.e., $\epsilon_{\min}$) are depicted in the insets of (c) and (d), respectively.

parameter as predicted by Eq. (12b). Experiments were also performed for a WVA of a small optical rotation effect [44]. The results confirmed imaginary and real WVAs of optical rotation $\alpha$, which were reflected in the ($\propto \alpha \cot \epsilon_{p/a}$) variation of the $\frac{V}{I}$ and $\frac{U}{Q}$ Stokes parameters, respectively (not shown here) [44]. The above results demonstrate real and imaginary WVAs of all the polarization anisotropy effects.

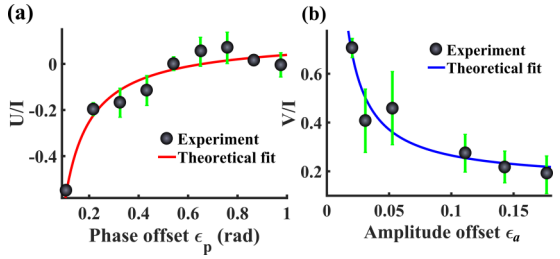


FIG. 4. Experimental results of real and imaginary WVAs of circular diattenuation ($\alpha = 0.012$). (a) Variation of $\frac{U}{I}$ Stokes parameter with $\epsilon_p$ (black circles) and corresponding theoretical fit to imaginary WVA ($\alpha \cot \epsilon_p$) (red line). (b) Variation of $\frac{V}{I}$ as a function of $\epsilon_a$ (black balls) and the corresponding real WVA fit ($\alpha \cot \epsilon_a$, blue line). Error bars represent standard deviations.

As we proceed further, it is worth noting that even though at first sight it may appear that WVAs of different polarization anisotropy effects are sometime manifested in the same Stokes vector elements, multiple polarimetry effects are in fact perfectly discernible through the real and imaginary weak-value measurement procedure and by a clever choice of the input polarization states, as is evident from Table I.

It is also pertinent to note that when multiple polarization effects are exhibited, the extraction and quantification of individual anisotropy parameters using conventional methods get confounded and necessitate cumbersome measurements such as the full 4×4 Mueller matrix measurement and its inverse analysis models that are often based on various assumptions and conditions. This interferometric WVA approach is potentially advantageous in this regard as it reduces the number of measurements and also obviates the need for the use of empirical inverse models for polarimetric quantification [7].

The experimental WVA curves and their weak-value fit for a given anisotropy effect provide the calibration curve for the quantification of any small anisotropy effect $\alpha$ of an unknown sample, which was validated by performing measurements for varying $\alpha$ (see details on calibration in Appendix B). We emphasize that in conventional polarimeters the sensitivity for the quantification of $\alpha$ is typically of the order of or lower than the sensitivity of the individual Stokes vector or Mueller matrix elements [8,9]. The most promising aspect of this interferometric WVA protocol, in this regard, is that one can achieve an amplification of the anisotropy parameter ($\alpha$) by a large WVA factor $\sim \cot \epsilon$. This essentially implies that one can, in principle, quantify an anisotropy parameter ($\alpha$) from the measurement of $\sim \cot \epsilon$ times larger Stokes parameters ($\sim \alpha \cot \epsilon$). In other words, for a given sensitivity of a Stokes polarimeter, using this interferometric WVA scheme, one can extract and quantify the polarization anisotropy parameter which is $\sim \epsilon$ times smaller than the sensitivity of measurement of a given Stokes parameter ($Q/I, U/I, V/I$). Since the WVA parameter $\epsilon$ is a small parameter ($\epsilon \ll 1$), this is equivalent to an enhancement of the sensitivity of a conventional Stokes polarimeter, which is used in our WVA experiments. We would, however, like to note that akin to all other WVA approaches, here also the large amplification of the polarization anisotropy parameter $\alpha$ comes at the expense of the intensity signal, which may also limit polarimetric sensitivity [34,45]. Thus, the actual benefit of this approach in terms of the enhancement of sensitivity of a conventional Stokes polarimeter remains to be rigorously evaluated. Here, we provide initial evidence of a sensitivity enhancement albeit for a relatively moderate magnitude of anisotropy $\alpha$.

For this purpose, we determine the sensitivity of measurement of the intensity normalized Stokes polarization parameters ($\frac{S_i}{I}$, $S_i = Q, U, V$) used in our interferometric WVA scheme, as this is relevant for the quantification of the polarization anisotropy parameter $\alpha$. The sensitivity here is limited by the corresponding intensity noise or uncertainty $\Delta(\frac{S_i}{I})$ (see Appendix C for the estimation of polarimetric sensitivity) [46]. As an illustrative example, in Fig. 5, we have shown the variation of the uncertainty in the intensity

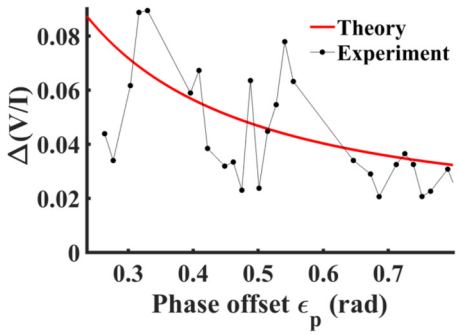


FIG. 5. Variation of the uncertainty in the intensity normalized Stokes parameter $\Delta(\frac{V}{I})$ with a varying $\epsilon_p$ parameter. Here, $\Delta(\frac{V}{I})$ is an indicator of the the sensitivity of $V/I$. The results are shown for the imaginary WVA of optical rotation ($\alpha = 0.035$). Black solid circles depict experimental sensitivity data and the corresponding theoretical prediction is shown by the solid red line.

normalized Stokes $V$ parameter $\Delta\frac{V}{I}$ with a varying phase offset parameter $\epsilon_p$ for the imaginary WVA of optical rotation. The results are shown for a value of $\alpha = 0.035$ rad. The theoretical values (shown by the red solid line) are generated using Eq. (C1). For this purpose, Eqs. (A16) and (A17) for the imaginary WVA of optical rotation are used. The corresponding experimental values of $\Delta(\frac{V}{I})$ are shown by the black solid circles in Fig. 5. Figure 5 implies that as $\epsilon_p \to 0$, the sensitivity of the determination of $(\frac{V}{I})$ deteriorates, i.e., uncertainty in $\Delta(\frac{V}{I})$ increases, which is expected, since overall the intensity falls as $\epsilon_p$ approaches zero. As noted above, this is a generic feature of any WVA approach [34,45]. It is pertinent to note here that WVA is not a null intensity detection technique as it uses the near orthogonal pre- and postselection of states corresponding to a small overlap $\epsilon_{a/p}$ between the pre- and postselection states [11,13]. Therefore, in WVA, there is an additional handle to optimize the amplification of any small physical parameter and the signal-to-noise ratio (SNR or sensitivity) by a judicial choice of the $\epsilon_{a/p}$ parameter. It has been earlier demonstrated that due to this and other related advantages, in general WVA outperforms comparable standard strong measurements [45]. Our interferometric WVA scheme of polarimetry is no exception in this regard. As is evident from Fig. 5, even though the sensitivity in the determination of $(\frac{V}{I})$ deteriorates [the uncertainty $\Delta(\frac{V}{I})$ increases] with decreasing $\epsilon_p$, the deterioration is not as drastic as the weak-value amplification factor $\sim \cot \epsilon_p$. Thus, an optimal range of $\epsilon_p$ (0.2–0.8) can be be worked out where one can obtain significant amplification with an acceptable level of SNR. Using the sensitivity analysis of Appendix C, a typical uncertainty (sensitivity) in the intensity normalized Stokes vector elements was determined to be ∼0.07. Using this, the typical sensitivity in estimating the optical rotation $\Delta\alpha$ was determined to be 0.008 rad for the range of $\epsilon_p$ (0.2–0.8). The sensitivity of the measurement of the same optical rotation ($\alpha \sim 0.035$ rad) using just the traditional Stokes polarization measurement was obtained to be ∼0.02 rad. These results provide evidence of the potential advantage and polarimetric sensitivity enhancement for the determination of optical rotation ($\alpha$) through the imaginary WVA of $(\frac{V}{I})$ by using the same Stokes polarization parameter measurement system in the interferometric WVA experimental embodiment.

We emphasize that this proof of concept of polarimetric sensitivity enhancement using the interferometric WVA approach is demonstrated using a dc Stokes polarimeter in our experimental configuration, which has an inherently low sensitivity (we could not go below $\alpha \sim 0.01$ rad due to this limitation). The principle is, however, expected to be valid for any conventional Stokes polarimeters irrespective of the specifics of the polarimeter. The initial results presented above on the enhancement of sensitivity are therefore quite promising and warrant further exploration towards the detection of polarization anisotropy below the conventional limit through the integration of this WVA scheme with relatively high-sensitivity Stokes polarimeters [7].

## V. CONCLUSION

In summary, using a simple yet profound philosophy of the interferometric realization of weak-value amplification of the polarization anisotropy effect, we have introduced and experimentally demonstrated an interesting and useful concept of a sample-measuring weak-value polarimeter. In this interferometric WVA approach, the pre- and postselection of states are obtained by the near destructive interference of two paths of an interferometer with slightly different polarization states of light due to the presence of a weak anisotropy effect in one path.

This approach enables the amplification and subsequent quantification of small magnitudes of all the sample polarization anisotropy effects in a single experimental embodiment. As other WVA protocols, this amplification is obtained at the cost of the intensity of the output signal. But the WVA approach also provides a handle to optimize the amplification of the polarization anisotropy effect and the polarimetric sensitivity by judiciously choosing the parameter $\epsilon_{a/p}$ that quantifies the overlap of pre- and postselected states. Real and imaginary WVAs of a given sample anisotropy effect manifest themselves in different characteristic Stokes vector elements, which evolve in orthogonal trajectories in the Poincaré sphere. This manifestation of the WVA of polarization anisotropy in the conjugate Stokes parameters has an intriguing quantum mechanical equivalence in the commutation relations of the analogous quantum Stokes polarization operators and in their uncertainty relations [43]. This WVA protocol may thus bear useful and interesting consequences in the studies of nontrivial polarization properties of light in quantum theory and in nonclassical polarization states. On practical grounds, the possibility of a significant enhancement of the sensitivity of polarization measurements using traditional Stokes polarimeters in the experimental embodiment of this WVA protocol is of general relevance for studying a wide range of weakly anisotropic materials and weak spin polarization optical effects for diverse applications [9]. Finally, the extension of this proposed sample-measuring weak-value polarimeter concept to other established domains of polarimetry such as in spectroscopic and imaging polarimetry remains to be explored. We are currently expanding our investigations in these directions by integrating interferometric spectroscopy and imaging and

microscopy methods [47,48] within the framework of a weak-value polarimeter.


## ACKNOWLEDGMENTS

We wish to acknowledge the support of the Indian Institute of Science Education and Research (IISER) Kolkata, an autonomous institute under the Ministry of Human Resource Development (MHRD), Government of India. Ankit Kumar Singh acknowledges the support of the Council of Scientific & Industrial Research (CSIR), India. We would like to acknowledge the Science and Engineering Research Board (SERB), Government of India for funding. Special thanks are given to Dr. Kamaraju Natarajan for experimental support.


## APPENDIX A: MANIFESTATION OF WVA OF DIFFERENT POLARIZATION ANISOTROPY EFFECTS IN CHARACTERISTIC STOKES VECTOR ELEMENTS

Here, we provide full expressions for the variations of the relevant Stokes vector elements with the small amplitude ($\epsilon_a$) and phase ($\epsilon_p$) offset parameters for real and imaginary (respectively) WVAs of linear and circular diattenuation and retardance effects. We define four parameters as listed below,

$$p_1 = \frac{1}{\sqrt{2}} + \frac{e^{\alpha}}{\sqrt{e^{2\alpha}+e^{-2\alpha}}}, \tag{A1a}$$

$$p_2 = \frac{1}{\sqrt{2}} - \frac{e^{\alpha}}{\sqrt{e^{2\alpha}+e^{-2\alpha}}}, \tag{A1b}$$

$$p_3 = \frac{1}{\sqrt{2}} - \frac{e^{-\alpha}}{\sqrt{e^{2\alpha}+e^{-2\alpha}}}, \tag{A1c}$$

$$p_4 = \frac{1}{\sqrt{2}} + \frac{e^{-\alpha}}{\sqrt{e^{2\alpha}+e^{-2\alpha}}}. \tag{A1d}$$

### 1. Stokes parameters for linear diattenuation (*x*-*y*)

As listed in Table I, the real and imaginary WVAs of a small linear diattenuation ($x$-$y$) effect are manifested in the Stokes vector elements $\frac{Q}{I}$ and $\frac{V}{I}$, respectively. The full expressions of the dependence of these Stokes parameters on $\epsilon_a$ and $\epsilon_p$ parameters are given as follows [8,9].

#### *a. Real WVA*

$$I = [\cos\epsilon_a p_2 + \sin\epsilon_a p_1]^2 + [\cos\epsilon_a p_3 + \sin\epsilon_a p_4]^2, \tag{A2}$$

$$Q = [\cos\epsilon_a p_2 + \sin\epsilon_a p_1]^2 - [\cos\epsilon_a p_3 + \sin\epsilon_a p_4]^2. \tag{A3}$$

The expressions given in Eqs. (A2) and (A3) in the limit $0 < \epsilon_a \ll 1$ lead to the WVA equation $\frac{Q}{I} \sim \alpha \cot\epsilon_a$ [Eq. (4)].

#### *b. Imaginary WVA*

Similarly, for imaginary WVA, the relevant Stokes parameters $(I, V)$ are given as, respectively,

$$I = \cos^2\epsilon_p p_2^2 + \sin^2\epsilon_p p_1^2 + \cos^2\epsilon_p p_3^2 + \sin^2\epsilon_p p_4^2, \tag{A4}$$

$$V = 2\cos\epsilon_p \sin\epsilon_p p_2 p_4 - 2\cos\epsilon_p \sin\epsilon_p p_1 p_3. \tag{A5}$$

Equations (A4) and (A5) yield the familiar WVA equation as $\frac{V}{I} \sim \alpha \cot\epsilon_p$ in a straightforward way in the limit $0 < \epsilon_p \ll 1$.

### 2. Stokes parameters for circular diattenuation

In a similar manner to the real and imaginary WVA of linear diattenuation ($x$-$y$), the electric fields corresponding to the circular diattenuation effect (provided in Table I) can be used to generate the Stokes parameters relevant to its WVA. The corresponding expressions are noted below [8,9].

#### *a. Real WVA*

$$I = [\cos\epsilon_a p_2 + \sin\epsilon_a p_1]^2 + [\cos\epsilon_a p_3 + \sin\epsilon_a p_4]^2, \tag{A6}$$

$$Q = [\cos\epsilon_a p_2 + \sin\epsilon_a p_1]^2 - [\cos\epsilon_a p_3 + \sin\epsilon_a p_4]^2. \tag{A7}$$

#### *b. Imaginary WVA*

$$I = \cos^2\epsilon_p p_2^2 + \sin^2\epsilon_p p_1^2 + \cos^2\epsilon_p p_3^2 + \sin^2\epsilon_p p_4^2, \tag{A8}$$

$$U = 2\cos\epsilon_p \sin\epsilon_p p_2 p_4 - 2\cos\epsilon_p \sin\epsilon_p p_1 p_3. \tag{A9}$$

### 3. Stokes parameters relevant to linear retardance

#### *a. Real WVA*

$$I = 4\left(\sin^2\frac{\alpha}{2}\cos^2\epsilon_a + \cos^2\frac{\alpha}{2}\sin^2\epsilon_a\right), \tag{A10}$$

$$V = 4\Bigg(\sin\alpha\cos\alpha\cos\epsilon_a\sin\epsilon_a - \sin\alpha\sin^2\frac{\alpha}{2}\cos^2\epsilon_a - \sin\alpha\cos^2\frac{\alpha}{2}\sin^2\epsilon_a\Bigg). \tag{A11}$$

#### *b. Imaginary WVA*

$$I = 2(1 - \cos 2\epsilon_p \cos\alpha), \tag{A12}$$

$$Q = 2\sin 2\epsilon_p \sin\alpha. \tag{A13}$$

### 4. Stokes parameters relevant to circular retardance

#### *a. Real WVA*

$$Q = (\cos\epsilon_a + \sin\epsilon_a)^2 + (\cos\epsilon_a - \sin\epsilon_a)^2\cos 2\alpha - 2\cos\alpha\cos 2\epsilon_a, \tag{A14}$$

$$U = \sin 2\alpha(\cos\epsilon_a - \sin\epsilon_a)^2 - 2\sin\alpha\cos 2\epsilon_a. \tag{A15}$$

#### *b. Imaginary WVA*

$$I = 2(1 - \cos\alpha\cos 2\epsilon_p), \tag{A16}$$

$$V = 2\sin\alpha\sin 2\epsilon_p. \tag{A17}$$

## APPENDIX B: CALIBRATION OF THE EXPERIMENTAL SYSTEM

Two different sets of calibrations are involved in this interferometric WVA scheme: (i) calibration of the interferometric WVA parameters, namely, the phase offset ($\epsilon_p$) and the amplitude offset ($\epsilon_a$) parameters in the interferometric setup, and (ii) calibration of the WVA curve of the different characteristic

Stokes vector elements encoding information on the different polarization anisotropy effects. Here, we briefly outline the procedure.

(1) For generating the experimental imaginary WVA curve, the values for the phase offset parameter $\epsilon_p$ at different spatial positions in the CCD image plane are calculated from the pixelwise spatial variation of the phase of the interference fringe. For this purpose, the phase difference of $2\pi$ between two consecutive destructive spatial positions of the fringe profile on the CCD plane was marked and the pixel corresponding to the destructive interference point was assigned a value of $\epsilon_p = 0$. The values of $\epsilon_p$ corresponding to consecutive CCD pixels away from the destructive interference point were subsequently obtained. For the given pixel dimension of 3.45 $\mu$m, the maximum resolution of the phase offset parameter (the minimum value of $\epsilon_p$ that can be used in the WVA scheme) in our experimental system was determined to be $\Delta\epsilon_p \sim 0.0132$ rad. The flatness in the spatial variation (or variation as a function of $\epsilon_p$) of the different characteristic Stokes vector elements in the absence of anisotropy effects ($\alpha = 0$) was ensured by performing blank (without sample) measurements. For generating the experimental real WVA curve, the amplitude offset parameter $\epsilon_a$ is determined by taking the ratio of intensity in the two arms of the interferometer. If the intensity is equal in both arms, then $\epsilon_a = 0$. Tuning the ND (see Fig. 1), we varied the intensity in one of the arms and determined $\epsilon_a$ in each case. For a given sensitivity of $\sim$0.001 $\mu$W of the detector used, the minimum value of the amplitude offset parameter in our experimental system is found to be $\Delta\epsilon_a \sim 0.01$. Once again, the flatness of the variation of the Stokes parameters with varying $\epsilon_a$ in the absence of the anisotropy effects was ensured by performing blank measurements.

(2) The variations of the different characteristic Stokes vector elements with varying $\epsilon_p/a$ parameters for imaginary and real WVAs (respectively) were generally fitted with the function $A\alpha \cot \epsilon_{p/a} + B$. Note that in an ideal case, the parameters $A$ and $B$ are expected to be unity and zero, respectively. These parameters were therefore determined by performing measurements on known magnitudes of the different polarization anisotropy effects ($\alpha$). The typical values for the $A$ and $B$ parameters of our experimental system were found to be in the range 0.80–1.08, and 0.002–0.010, respectively. Several factors contribute to these variations, e.g., due to nonideal polarization optical components (polarizers and wave plates), slight misalignments, and other experimental imperfections, etc. Thus, the above-mentioned WVA fits (with known $A$ and $B$ experimental parameters for respective anisotropy effects) provide the calibration WVA curve of the experimental system for the measurement of any unknown anisotropy parameter $\alpha$. The linearity of the values of $\alpha$ estimated from the WVA fitting, with a varying magnitude of the input anisotropy parameter, was also confirmed by performing multiple measurements.

## APPENDIX C: SENSITIVITY ESTIMATION

In the context of the quantification of polarization anisotropy $\alpha$, we are interested in the sensitivity of determining the intensity normalized Stokes parameters ($\frac{S_i}{I}$, $S_i = Q, U, V$, and $I$ is the total intensity, the sum of intensities of any two orthogonal polarizations). The sensitivity of measurement of ($\frac{S_i}{I}$) used in our interferometric WVA scheme is limited by the noise or uncertainty $\Delta(\frac{S_i}{I})$, i.e., a smaller $\Delta(\frac{S_i}{I})$ corresponds to better sensitivity. In this regard, the signal-to-noise ratio (SNR) of the normalized Stokes parameters can be formally defined as $(\frac{S_i}{I})_{\text{SNR}} = \frac{\frac{S_i}{I}}{\Delta(\frac{S_i}{I})}$. Here, the uncertainty $\Delta(\frac{S_i}{I})$ primarily arises due to the photon shot noise and the readout noise of the detector. For an un-normalized Stokes parameter $S$, the corresponding noise or uncertainty is $\Delta S_i \sim \sqrt{I + 2R^2}$, where $R$ is the readout noise [46]. The readout noise of our experimental detector was determined from the recorded images in the camera in a dark condition and the value was estimated to be 0.2. Thus, in our case, the overall noise was mainly shot-noise limited, i.e., $\Delta S_i \sim \sqrt{I}$. Based on these definitions and by using a standard error propagation method, the uncertainty of the normalized Stokes parameters $\Delta(\frac{S_i}{I})$ can be obtained as [49]

$$\Delta\left(\frac{S_i}{I}\right) = \frac{\frac{S_i}{I}}{\left(\frac{S_i}{I}\right)_{\text{SNR}}} = \frac{\Delta S_i (I + S_i)}{I^2}. \tag{C1}$$

The above equation was used to determine the sensitivity of normalized Stokes parameter measurements $\Delta(\frac{S_i}{I})$ and the resultant sensitivity of determination of all the sample polarization anisotropy effects $\Delta\alpha$ of our interferometric WVA polarimeter. Illustrative results of the sensitivity analysis for the imaginary WVA of optical rotation are presented in Fig. 5.


[1] K. Y. Bliokh, A. Niv, V. Kleiner, and E. Hasman, Geometrodynamics of spinning light, Nat. Photon. **2**, 748 (2008).

[2] K. Y. Bliokh, D. Smirnova, and F. Nori, Quantum spin Hall effect of light, Science **348**, 1448 (2015).

[3] A. Aiello, P. Banzer, M. Neugebauer, and G. Leuchs, From transverse angular momentum to photonic wheels, Nat. Photon. **9**, 789 (2015).

[4] D. Lin, P. Fan, E. Hasman, and M. L. Brongersma, Dielectric gradient metasurface optical elements, Science **345**, 298 (2014).

[5] M. Pal, S. Saha, B. S. Athira, S. D. Gupta, and N. Ghosh, Experimental probe of weak-value amplification and geometric phase through the complex zeros of the response function, Phys. Rev. A **99**, 032123 (2019).

[6] J. J. G. Pérez and R. Ossikovski, *Polarized Light and the Mueller Matrix Approach* (CRC Press, Boca Raton, FL, 2016).

[7] R. Azzam, Stokes-vector and Mueller-matrix polarimetry, J. Opt. Soc. Am. A **33**, 1396 (2016).

[8] E. Collett, *Polarized Light: Fundamentals and Applications* (CRC Press, Boca Raton, FL, 1993), Vol. 36.

[9] S. D. Gupta, N. Ghosh, and A. Banerjee, *Wave Optics: Basic Concepts and Contemporary Trends* (CRC Press, Boca Raton, FL, 2015).

[10] B. S. Athira, M. Pal, S. Mukherjee, J. Mishra, D. Nandy, and N. Ghosh, Single-shot measurement of the space-varying polarization state of light through interferometric quantification of the geometric phase, Phys. Rev. A **101**, 013836 (2020).

[11] Y. Aharonov, D. Z. Albert, and L. Vaidman, How the Result of a Measurement of a Component of the Spin of a Spin-1/2 Particle can Turn Out to be 100, Phys. Rev. Lett. **60**, 1351 (1988).

[12] A. K. Singh, S. Saha, S. D. Gupta, and N. Ghosh, Transverse spin in the scattering of focused radially and azimuthally polarized vector beams, Phys. Rev. A **97**, 043823 (2018).

[13] I. Duck, P. M. Stevenson, and E. Sudarshan, The sense in which a "weak measurement" of a spin-1/2 particle's spin component yields a value 100, Phys. Rev. D **40**, 2112 (1989).

[14] A. G. Kofman, S. Ashhab, and F. Nori, Nonperturbative theory of weak pre- and post-selected measurements, Phys. Rep. **520**, 43 (2012).

[15] J. Dressel, M. Malik, F. M. Miatto, A. N. Jordan, and R. W. Boyd, Colloquium: Understanding quantum weak values: Basics and applications, Rev. Mod. Phys. **86**, 307 (2014).

[16] N. Ritchie, J. G. Story, and R. G. Hulet, Realization of a Measurement of a "Weak Value", Phys. Rev. Lett. **66**, 1107 (1991).

[17] O. Hosten and P. Kwiat, Observation of the spin Hall effect of light via weak measurements, Science **319**, 787 (2008).

[18] O. S. Magaña-Loaiza, M. Mirhosseini, B. Rodenburg, and R. W. Boyd, Amplification of Angular Rotations using Weak Measurements, Phys. Rev. Lett. **112**, 200401 (2014).

[19] X.-Y. Xu, Y. Kedem, K. Sun, L. Vaidman, C.-F. Li, and G.-C. Guo, Phase Estimation with Weak Measurement using a White Light Source, Phys. Rev. Lett. **111**, 033604 (2013).

[20] P. B. Dixon, D. J. Starling, A. N. Jordan, and J. C. Howell, Ultrasensitive Beam Deflection Measurement via Interferometric Weak Value Amplification, Phys. Rev. Lett. **102**, 173601 (2009).

[21] M. Asano, K. Bliokh, Y. Bliokh, A. Kofman, R. Ikuta, T. Yamamoto, Y. Kivshar, L. Yang, N. Imoto, Ş. Özdemir *et al.*, Anomalous time delays and quantum weak measurements in optical micro-resonators, Nat. Commun. **7**, 1 (2016).

[22] H. Kobayashi, K. Nonaka, and Y. Shikano, Stereographical visualization of a polarization state using weak measurements with an optical-vortex beam, Phys. Rev. A **89**, 053816 (2014).

[23] S. Nechayev, M. Neugebauer, M. Vorndran, G. Leuchs, and P. Banzer, Weak Measurement of Elliptical Dipole Moments by *C*-Point Splitting, Phys. Rev. Lett. **121**, 243903 (2018).

[24] I. Shomroni, O. Bechler, S. Rosenblum, and B. Dayan, Demonstration of Weak Measurement Based on Atomic Spontaneous Emission, Phys. Rev. Lett. **111**, 023604 (2013).

[25] A. K. Singh, S. K. Ray, S. Chandel, S. Pal, A. Gupta, P. Mitra, and N. Ghosh, Tunable Fano resonance using weak-value amplification with asymmetric spectral response as a natural pointer, Phys. Rev. A **97**, 053801 (2018).

[26] J. S. Lundeen, B. Sutherland, A. Patel, C. Stewart, and C. Bamber, Direct measurement of the quantum wavefunction, Nature (London) **474**, 188 (2011).

[27] A. Palacios-Laloy, F. Mallet, F. Nguyen, P. Bertet, D. Vion, D. Esteve, and A. N. Korotkov, Experimental violation of a Bell's inequality in time with weak measurement, Nat. Phys. **6**, 442 (2010).

[28] S. Kocsis, B. Braverman, S. Ravets, M. J. Stevens, R. P. Mirin, L. K. Shalm, and A. M. Steinberg, Observing the average trajectories of single photons in a two-slit interferometer, Science **332**, 1170 (2011).

[29] J. Z. Salvail, M. Agnew, A. S. Johnson, E. Bolduc, J. Leach, and R. W. Boyd, Full characterization of polarization states of light via direct measurement, Nat. Photon. **7**, 316 (2013).

[30] L. Luo, L. Xie, J. Qiu, X. Zhou, X. Liu, Z. Li, Y. He, Z. Zhang, and H. Sun, Simultaneously precise estimations of phase and amplitude variations based on weak-value amplification, Appl. Phys. Lett. **114**, 111104 (2019).

[31] Y. Xu, L. Shi, T. Guan, S. Zhong, X. Zhou, D. Li, C. Guo, Y. Yang, X. Wang, Z. Li *et al.*, Multifunctional weak measurement system that can measure the refractive index and optical rotation of a solution, Appl. Phys. Lett. **114**, 181901 (2019).

[32] G. Pryde, J. O'Brien, A. White, T. Ralph, and H. Wiseman, Measurement of Quantum Weak Values of Photon Polarization, Phys. Rev. Lett. **94**, 220405 (2005).

[33] B. de Lima Bernardo, S. Azevedo, and A. Rosas, Ultrasmall polarization rotation measurements via weak value amplification, Phys. Lett. A **378**, 2029 (2014).

[34] C. Ferrie and J. Combes, Weak Value Amplification is Suboptimal for Estimation and Detection, Phys. Rev. Lett. **112**, 040406 (2014).

[35] M. Berry and P. Shukla, Pointer supershifts and superoscillations in weak measurements, J. Phys. A: Math. Theor. **45**, 015301 (2011).

[36] Z. Zhu, D. Hay, Y. Zhou, A. Fyffe, B. Kantor, G. S. Agarwal, R. W. Boyd, and Z. Shi, Single-Shot Direct Tomography of the Complete Transverse Amplitude, Phase, and Polarization Structure of a Light Field, Phys. Rev. Applied **12**, 034036 (2019).

[37] G. Puentes, N. Hermosa, and J. P. Torres, Weak Measurements with Orbital-Angular-Momentum Pointer States, Phys. Rev. Lett. **109**, 040401 (2012).

[38] M. Iinuma, Y. Suzuki, G. Taguchi, Y. Kadoya, and H. F. Hofmann, Weak measurement of photon polarization by back-action-induced path interference, New J. Phys. **13**, 033041 (2011).

[39] H. Rhee, I. Eom, S.-H. Ahn, K.-H. Song, and M. Cho, Chiroptical signal enhancement in quasi-null-polarization-detection geometry: Intrinsic limitations, Phys. Rev. A **91**, 053839 (2015).

[40] J. Dziewior, L. Knips, D. Farfurnik, K. Senkalla, N. Benshalom, J. Efroni, J. Meinecke, S. Bar-Ad, H. Weinfurter, and L. Vaidman, Universality of local weak interactions and its application for interferometric alignment, Proc. Natl. Acad. Sci. USA **116**, 2881 (2019).

[41] J. Von Neumann, *Mathematical Foundations of Quantum Mechanics: New Edition* (Princeton University Press, Princeton, NJ, 2018).

[42] D. Han, Y. Kim, and M. E. Noz, Stokes parameters as a Minkowskian four-vector, Phys. Rev. E **56**, 6065 (1997).

[43] W. P. Bowen, N. Treps, R. Schnabel, and P. K. Lam, Experimental Demonstration of Continuous Variable Polarization Entanglement, Phys. Rev. Lett. **89**, 253601 (2002).

[44] S. Guchhait, B. S. Athira, N. Modak, J. K. Nayak, A. Panda, M. Pal, and N. Ghosh, Natural weak value amplification in Fano

resonance and giant Faraday rotation in magneto-plasmonic crystal, Sci. Rep. **10**, 1 (2020).

[45] J. Harris, R. W. Boyd, and J. S. Lundeen, Weak Value Amplification can Outperform Conventional Measurement in the Presence of Detector Saturation, Phys. Rev. Lett. **118**, 070802 (2017).

[46] R. Perkins and V. Gruev, Signal-to-noise analysis of Stokes parameters in division of focal plane polarimeters, Opt. Express **18**, 25815 (2010).

[47] F. Huth, M. Schnell, J. Wittborn, N. Ocelic, and R. Hillenbrand, Infrared-spectroscopic nanoimaging with a thermal source, Nat. Mater. **10**, 352 (2011).

[48] P. M. Hinz, J. R. P. Angel, W. F. Hoffmann, D. W. McCarthy, P. C. McGuire, M. Cheselka, J. L. Hora, and N. J. Woolf, Imaging circumstellar environments with a nulling interferometer, Nature (London) **395**, 251 (1998).

[49] P. R. Bevington and D. K. Robinson, *Data Reduction and Error Analysis* (McGraw-Hill, New York, 2003).